FLOW REATTACHMENT ON WINGS IN PITCH-DOWN MOTION

Lars E. Ericsson
Engineering Consultant
Mt. View, California, USA

Abstract

An analysis has been performed of existing theoretical and experimental results to determine the flow physics responsible for the observed delay of flow reattachment to a negative flow incidence in a modestly rapid pitch-down motion of an airfoil. It is found that the responsible flow physics are essentially the same as those causing dynamic overshoot of static lift maximum in pitch-up motions, i. e. the accelerated flow and moving wall effects. The analysis shows that the dominant role played by the moving wall effect during pitch-down motions is in agreement with existing experimental results for a rotating circular cylinder. Applying the moving wall effect, measured through the Magnus lift on a rotating circular cylinder, to an airfoil describing pitch-down motions produces predictions that are in good agreement with experimental results. A thorough understanding of this moving wall effect is required for prediction of the high-alpha unsteady aerodynamics of advanced aircraft.

Nomenclature

b	wing span
c	reference length, airfoil chord
f	oscillation frequency
K_1	constant in Eq. (2)
K_2	constant in Eq. (3)
l'	sectional lift, coefficient $c_l = l' / (\rho_\infty U_\infty^2/2)\, c$
l	rolling moment, coefficient $C_l = l / (\rho_\infty U_\infty^2/2)\, S\, b$
M	free stream Mach number
n	sectional normal force, coefficient $c_n = n / (\rho_\infty U_\infty^2/2)\, c$
p	roll rate
r_N	airfoil nose radius
Re	Reynolds number, $Re = U_\infty c/\nu_\infty$
S	reference area, projected wing area
t	time
U	velocity
x	distance from the leading edge
z	translatory coordinate
α	angle of attack
α_0	mean angle of attack
Δ	amplitude or increment
ζ	dimensionless z-coordinate, $\zeta = z/c$
θ	perturbation in pitch
ρ_N	dimensionless nose radius, $\rho_N = r_N/c$
ρ_∞	air density
σ	inclination of roll axis
ϕ	roll angle
ν	kinematic viscosity
ω	angular frequency, $\omega = 2\pi f$
$\bar{\omega}$	dimensionless frequency, $\bar{\omega} = \omega c/U_\infty$
ξ	dimensionless x-coordinate, $\xi = x/c$
$\Delta\zeta$	dimensionless z-amplitude, $\Delta\zeta = \Delta z/c$

Subscripts

a	accelerated flow
CG	center of gravity or rotation
d	decelerated flow
h	hysteresis
ir	incipient reattachment
r	reattachment
s	separation
N	nose
w	wake
W	wall
1,2	numbering subscripts

∞   free stream conditions

Derivative symbols

$\dot\theta = \partial\theta/\partial t$; $C_{lp} = \partial C_l/\partial(pb/2U_\infty)$; $c_{l\alpha} = \partial c_l/\partial\alpha$

Introduction

The experimental results obtained by Niven and Galbraith[1] for down-ramp motion of airfoils from fully stalled conditions (Fig. 1) beg for an explanation of the underlying flow physics. A satisfactory understanding of these dynamic characteristics is critical for prediction of wing rock of aircraft with wings of moderate sweep[2], such as the Gnat aircraft[3] (Fig.2) or the X-29A[4] (Fig. 3). The wing rock is caused by the negative damping-in-plunge generated by the airfoil section on the rocking wing at penetration of the static stall region[2], as is demonstrated by the experimental results presented by Liiva et al[5] (Fig. 4). Dynamic stall concepts developed earlier[6] will be applied to determine the flow physics behind the unusual experimental results in Fig. 1.

Analysis

The overshoot of the static stall angle on an airfoil in pitch-up motion has two components[6], $\Delta\alpha_w$ and $\Delta\alpha_s$. $\Delta\alpha_w$ is a pure time lag effect, causing the airfoil to attain the static force after a time increment Δt at an angle of attack $\alpha(t + \Delta t)$ that is larger than the static value by $\Delta\alpha_w \approx \dot\alpha\,\Delta t$. The other component, $\Delta\alpha_s$, generates a change of the force vector from its static value (whereas the component $\Delta\alpha_w$ only generates a phase lag of the unchanged static force vector), causing an increase of the lift maximum by $\Delta c_{l\,max} \approx c_{l\alpha}\Delta\alpha_s$. This results from the improvement of the boundary layer characteristics, generated by the pitch-up motion of the airfoil through accelerated flow and moving wall effects[6].

From Ref. 6 one obtains the following definition of the change $\Delta\alpha_s$ from the static stall angle α_s.

$$\Delta\alpha_s = \Delta\alpha_{s1} + \Delta\alpha_{s2} \qquad (1)$$

In Eq. (1) the component $\Delta\alpha_{s1}$ is generated by the accelerated-flow effect on the ambient pressure-gradient time history. It is only determined by the rate of change of the angle of attack and can be written

$$\Delta\alpha_{s1} = K_1\,\dot\alpha c/U_\infty \qquad (2)$$

The other component, $\Delta\alpha_{s2}$, is generated by the LE-jet effect (Fig. 5). In a first approximation, $\Delta\alpha_{s2}$ is proportional to the LE-plunging velocity $\dot z_{LE}$, i.e.

$$\Delta\alpha_{s2} = -K_2\,\dot z_{LE}/U_\infty \qquad (3)$$

That is, for an airfoil pitching around ξ_{CG}

$$\Delta\alpha_s = \Delta\alpha_{s1} + \Delta\alpha_{s2} = K\,\dot\alpha c/U_\infty \qquad (4a)$$

$$K = K_1 + K_2\,\xi_{CG} \qquad (4b)$$

Dynamic test results for the NACA-0012 airfoil[5] gave a value K = 3.0 for ξ_{CG} = 0.25. Equations (4) show that the dynamic stall overshoot of the static maximum lift or normal force should increase with increasing ξ_{CG}, in agreement with experimental results[7] (Fig. 6). Figure 7 shows that when plotted as a function of the reduced frequency $\bar\omega$, these experimental results for 6 deg. amplitude oscillations of the NACA-0012 airfoil exhibit the same highly nonlinear behavior as those of Carr et al for 10 deg. amplitude oscillations[8] (Fig. 8). It is shown in Ref. 9 that the nonlinearity is in large part caused by the effect of the "spilled" leading-edge vortex. In earlier analysis of dynamic test results for the NACA-0012 airfoil[10] it was found that $K_2 \approx 2\,K_1$ in Eqs. (4). That is,

$$\Delta\alpha_s \approx K_1\,(1 + 2\,\xi_{CG})\,\dot\alpha c/U_\infty \qquad (5)$$

Figure 9 shows that when plotted in the normalized form $\Delta c_{n\,max}\,/\,(1 + 2\,\xi_{CG})$, the experimental data from Fig. 7 tend to collapse. For ξ_{CG} = 0.37 and 0.50 the collapse is complete, including the envelopes of the data spread. Although the normalized experimental results for ξ_{CG} = 0.25 fall somewhat below those for ξ_{CG} = 0.37 and 0.50, when considering the data scatter for each ξ_{CG} the collapse of the experimental results is satisfactory. Thus, one can represent $\Delta\alpha_s$ by Eq. (5), where $K_1 = K_a$ is the accelerated flow effect.

Flow Reattachment.

Analysis of experimental results[6,10] has indicated that also the dynamic undershoot $\Delta\alpha_r$ of static flow reattachment is proportional to the dimensionless pitch rate $\dot\alpha c/U_\infty$. Thus, Eq. (5) can represent $\Delta\alpha_r$ when written in the following form

$$\Delta\alpha_r \approx K_d\,(1 + 2\,\xi_{CG})\,\dot\alpha c/U_\infty \qquad (6)$$

where K_d is the decelerated flow effect.

In Fig. 10 is shown how the flow reattachment characteristics for a NACA-0015 airfoil varied with $\dot\alpha c/U_\infty$ in the experiment performed by Niven and Gailbraith[1]. Figure 11 shows that the angle of attack for flow reattachment, as determined from the experimental results in Fig. 10, is linearly dependent upon $\dot\alpha c/U_\infty$, in agreement with Eq. (6). That the final reattachment at α_r is not always preceded by an incipient reattachment process starting at α_{ir} is apparent from the experimental results[11] in Fig. 12. The figure shows also the presence of static hysteresis (α_h) for the flow reattachment, explaining the initial, very sharp drop of α_r in Fig. 11.

According to Figs. 11 and 12 one can express the flow reattachment angle of attack as follows with the aid of Eq. (6).

$$\alpha_r = \alpha_s - \alpha_h + K_d\,(1 + 2\,\xi_{CG})\,\dot\alpha c/U_\infty \qquad (7)$$

It remains to determine the value of K_d in Eq. (7).

A rotating circular cylinder represents a well-known form of moving wall effects, which is used in Fig. 5 to illustrate the leading-edge jet effect on a pitching or plunging airfoil. Figure 13 shows the Magnus lift measured by Swanson[12] on a rotating circular cylinder. In the laminar, subcritical case (Fig. 13a), the Magnus lift is generated mainly by the downstream moving wall effect on the top side, which moves the flow separation from the subcritical towards the supercritical position. On

the bottom side the flow separation is occurring forward of the lateral meridian already in the static case, and the upstream moving wall effect does not have much leverage for its separation-promoting action. However, in the turbulent, supercritical case (Fig. 13b), the situation is reversed. The main effect is that of the upstream moving wall effect on the bottom side, which promotes flow separation, moving it from the supercritical towards the subcritical position. The downstream moving wall effect on the top side has very limited possibility to cause further delay of the already supercritical flow separation. Thus, the difference in Magnus lift between laminar and turbulent flow conditions is mainly the result of the difference between the capability of the moving wall effect to delay laminar flow separation and promote turbulent separation. The difference in Magnus lift slopes, the laminar one being only 3/8 of the turbulent one, reflects the fact that it is much more difficult to delay than to promote flow separation.

It is well established that the moving wall effect is mainly affecting the initial boundary layer build-up close to the flow stagnation point[13,14]. Thus, it is valid to compare the moving wall effects on a rotating cylinder[12] (Fig. 13) with those on a pitching or plunging airfoil[6,10] (Fig. 5). Therefore, the moving wall effects on the initial build-up of the laminar boundary layer is very similar in Figs. 5 and 13. It does, of course, not follow that the effect on the downstream flow separation must also be similar. However, for lack of other applicable experimental results the 8 to 3 ratio between separation-promoting and separation-delaying moving wall effects will be used to compare $\Delta\alpha_r$ to $\Delta\alpha_s$, Eqs. (6) and (5), respectively. Combining Eqs. (4) and (5), where $K_1 = K_a = 2$, with Eq. (6), where it is assumed that $K_d \approx 8 K_a /3$, one obtains for $\xi_{CG} = 0.25$

$$\Delta\alpha_r = 4 K_a \dot{\alpha}c/U_\infty \qquad (8)$$

That is, with $K_a = 2$ one obtains $\Delta\alpha_r = 8 \dot{\alpha}c/U_\infty$. The experimental results in Fig. 11 give $\Delta\alpha_r \approx 13 \dot{\alpha}c/U_\infty$. One would expect that K_d would be of larger magnitude for NACA-0015 than for NACA-0012 because of the difference in nose radii[15], $\rho_N = 0.0248$ compared to $\rho_N = 0.0158$. The analysis in Ref. 15 derives the functional relationship $K_a(\rho_N)$. In the present case the analysis gives $K_a(0.0248)/K_a(0.0158) = 1.86$. As $K_a(0.0158) = 2$ for NACA-0012, Eq. (8), one obtains for the NACA-0015 airfoil $\Delta\alpha_r \approx 15 \dot{\alpha}c/U_\infty$, a value embarrassingly close to the experimental value in Fig. 11. The experimental results[1] in Fig. 14 show the expected[15] large effect of increasing nose radius. The figure also shows the large effect of camber (compare NACA-0015 with NACA-23012B). The camber increases the effective nose radius through its nose-droop effect, which has been shown to be large, able to increase $\Delta\alpha_s$ substantially[16](Fig. 15). It can, therefore, be expected to have the large effect on $\Delta\alpha_r$ exhibited in Fig. 14.

Plunging Oscillations

Figure 5 illustrates the fact that for a pitching airfoil $\Delta\alpha_{s1}$ and $\Delta\alpha_{s2}$ are additive, as is shown in Eqs. (4), but are opposing each other for a plunging airfoil. That is,

$$\Delta\alpha_{s1} = K_1 \dot{z}_{LE}/U_\infty \qquad (9a)$$

$$\Delta\alpha_{s2} = - K_2 \dot{z}_{LE}/U_\infty \qquad (9b)$$

In the case of the pitching oscillations, $K_2 = 2 K_a$, whereas for plunging oscillations it is $K_2 = 2 K_d$, where $K_d \approx 8 K_a/3$. With $K_a \approx 2.0$ for the NACA-0012 airfoil, the value for K_d is $K_d \approx 16/3$, giving $K_2 = 2 K_d = 32/3$. Thus, Eqs. (9) define $\Delta\alpha_s = \Delta\alpha_{s1} + \Delta\alpha_{s2}$ as follows

$$\Delta\alpha_s = (K_1 - K_2) \dot{z}_{LE}/U_\infty \approx - (26/3) \dot{z}_{LE}/U_\infty \quad (10)$$

Thus, for a plunging airfoil the moving wall effect dominates, and promotes dynamic stall, whereas stall is delayed for a pitching airfoil. As a consequence, plunging oscillations become undamped when stall occurs[5] (Fig. 4), leading to the wing rock experienced by the Gnat and X-29A aircraft[3,4] (Figs. 2 and 3). For the rolling wing, the effective angle of attack varies as follows with the roll angle ϕ, for the roll-axis-inclination σ

$$\alpha(\phi) = \tan^{-1} (\tan \sigma \cos \phi) \qquad (11)$$

When $\alpha(\phi) < \alpha_{reatt.}$, the plunging wing section starts generating positive damping. At the limit-cycle amplitude this includes a sufficient part of the oscillation cycle away from $\phi = 0$ to result in zero net damping. Equation (11) shows how $\alpha(\phi)$ increases with increasing inclination σ of the roll axis, requiring higher and higher roll angle ϕ to reach the condition $\alpha(\phi) < \alpha_{reatt.}$. The fast increase of the wing-rock amplitude with increasing angle of attack for X-29A (Fig. 3b) reflects this effect of increasing σ.

Scaling Problems

When trying to apply results such as those in Figs. 1, 4, 6, and 10 to full-scale flight, one always has to account for the differences in Reynolds number[17]. This scaling problem is complicated greatly by the always present large effects of compressibility[18]. This is demonstrated by the wing rock results for the Gnat aircraft[3] (Fig. 2). The wing rock starts at lower and lower angle of attack for increasing subsonic Mach number. This is in agreement with the decreasing stall angle with increasing Mach number illustrated by the decreasing maximum lift with increasing Mach number[15,19,20] (Fig. 16). It is shown in Ref. 15 that the data trend in Fig. 16 is the result of the decrease of the effective nose radius $\rho_N = r_N/c$ with increasing Mach number due to the effect of compressibility, resulting in the predicted data trend shown by the solid line in Fig. 16.

Conclusions

An analysis has shown that the at first surprising experimental results obtained for a ramp-down motion, showing that flow reattachment can be delayed to negative angles of attack, are in good agreement with expectations based upon the existing experimental data base for dynamic airfoil stall and the Magnus lift measured on a rotating circular cylinder.

References

1. Niven, A. J. and Galbraith, R. A. McD., "Experiments on the Establishment of Fully Attached Airfoil Flow From the Fully Stalled Condition During Ramp-Down Motions," ICAS Paper 90-3.4.3, Sept. 1990.

2. Ericsson, L. E., "Various Sources of Wing Rock," Journal of Aircraft, Vol. 27, June 1990, pp. 488-494.

3. Ross, A. J., "Lateral Stability at High Angles of Attack, Particularly Wing Rock," Paper 10, AGARD-CP-260, 1978.

4. Fratello, D. J., Croom, M. A., Nguyen, L. T., and Domack, C. S., " Use of the Updated NASA Langley Radio-Controlled Drop Model Technique for High-Alpha Studies of X-29A Configuration," AIAA Paper 87-2559, Aug. 1987 (Fig. 3b was only shown in the oral presentation).

5. Liiva, J., Davenport, F. J., Gray, L., and Walton, I. C., "Two-Dimensional Tests of Airfoils Oscillating Near Stall," TR 68-13, U. S. Army Aviation Labs, Fort Eustis, VA, April 1968.

6. Ericsson, L. E. and Reding, J. P., "Fluid Mechanics of Dynamic Stall, Part I-Unsteady Flow Concepts," Journal of Fluids and Structures, Vol. 2, Jan. 1988, pp. 1-33.

7. Windsor, R. I., "Measurements of Aerodynamic Forces on an Oscillating Airfoil," TR-69-98, US Army Aviation Labs, Fort Eustis, Virginia, March 1970.

8. Carr, L. W., McAlister, K. W., and McCroskey, W. J., "Analysis of the Development of Dynamic Stall Based on Oscillating Airfoil Experiments," NASA TN D-8382, Jan. 1977.

9. Ericsson, L. E. and Reding, J. P., "Dynamic Stall at High Frequency and Large Amplitude," Journal of Aircraft, Vol. 17, March 1980, pp. 136-142.

10. Ericsson, L. E. and Reding, J. P., "Dynamic Stall Analysis in Light of Recent Numerical and Experimental Results," Journal of Aircraft, Vol. 13, April 1976, pp. 248-255.

11. Critzos, C. C., Heyson, H. H., and Boswinkle, R. W., Jr., "Aerodynamic Characteristics of NACA-0012 Airfoil Section at Angles of Attack from $0°$ to $180°$," NACA TN 3361 (1955).

12. Swanson, W. M., "The Magnus Effect: A Summary of Investigations to Date," Journal of Basic Engineering, Vol. 83, 1961, pp. 461-470.

13. Dwyer, H. A. and McCroskey, W. J., "Oscillating Flow Over a Cylinder at Large Reynolds Number," Journal of Fluid Mechanics, Vol. 61, Pt. 4, 1973, pp. 753-767.

14. Ericsson, L. E., "Circular Cylinder Response to Karman Vortex Shedding," Journal of Aircraft, Vol. 25, Sept. 1988, pp. 769-775.

15. Ericsson, L. E. and Reding, J. P., "Stall Flutter Analysis," Journal of Aircraft, Vol. 10, Jan. 1973, pp. 5-13.

16. Kelly, J. A., "Effect of Modification to the Leading-Edge Region on the Stalling Characteristics of NACA 63_1-012 Airfoil Section," NACA TN 2228 (1950).

17. Ericsson, L. E., "Effects of Transition on Wind Tunnel Simulation of Vehicle Dynamics," Prog. Aerospace Sci., Vol. 27, 1990, pp. 121-144.

18. Ericsson, L. E., "The Problem of Dynamic Stall Simulation Revisited," AIAA Paper 93-0091, Jan. 1993.

19. Harper, P. W. and Flanigan, R. E., "Investigation of the Variation of Maximum Lift for a Pitching Airplane Model and Comparison with Flight Results," NACA TN 1734 (1948).

20. Harper, P. W. and Flanigan, R. E., "The Effect of Rate of Change of Angle of Attack on the Maximum Lift of a Small Model," NACA TN 2061 (1949).
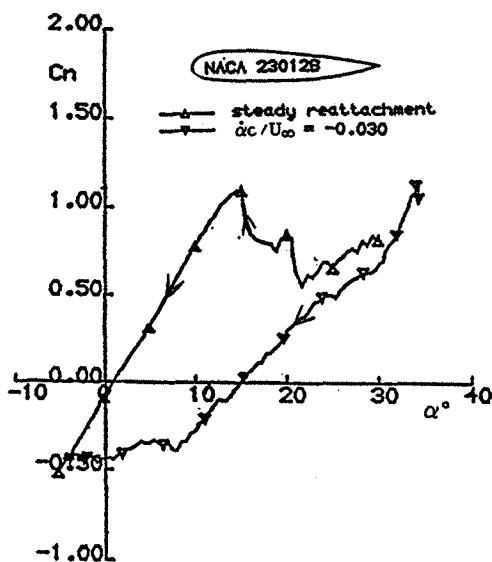
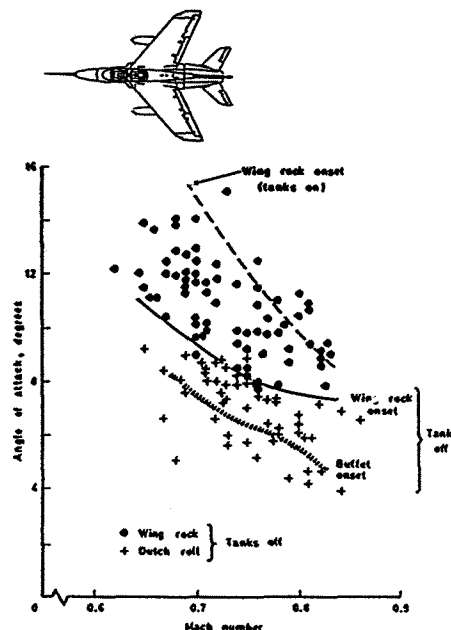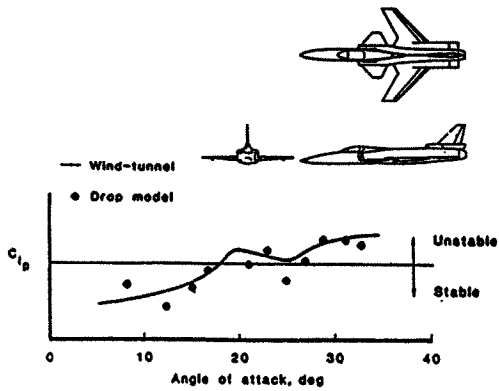Fig. 1. Effect of a pitch-down ramp of $\dot{\alpha}c/U_\infty = -0.03$ on airfoil normal force[1].
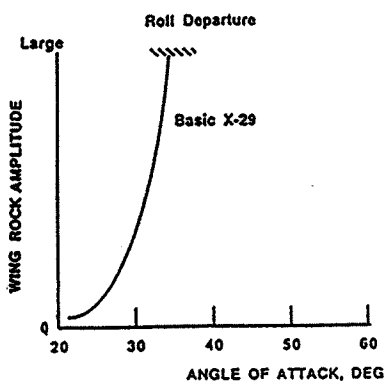

Fig. 2. Wing rock of the Gnat aircraft[3].

1157

a) Roll damping of X-29A models

b) Wing rock characteristics of the X-29 aircraft
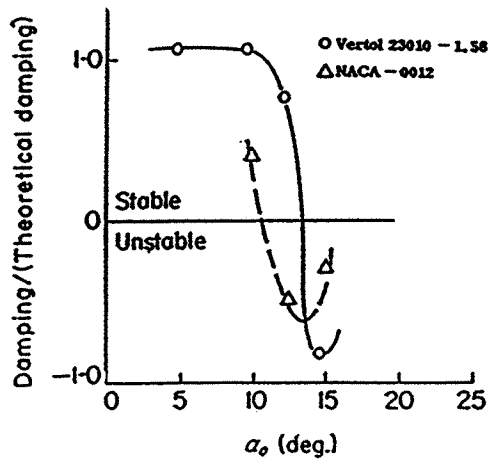
Fig. 3.   Wing rock of the X-29 A aircraft[4].

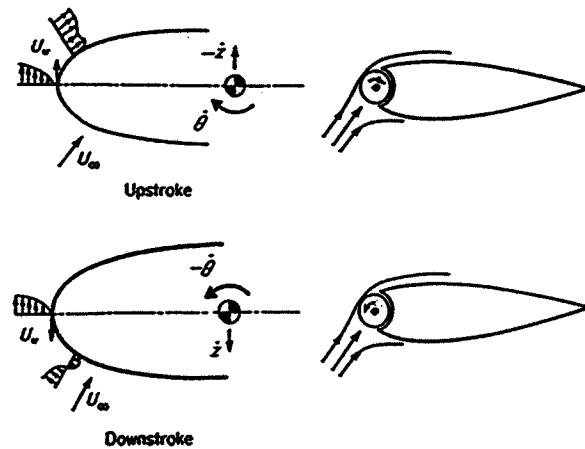Fig. 4.   Airfoil damping-in-plunge at M = 0.4, $\bar{\omega}$ = 0.136, and $\Delta\zeta$ = 0.153 (Ref. 5).

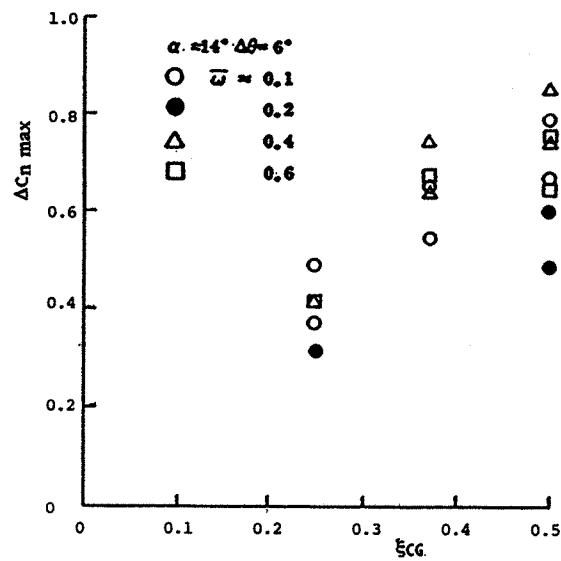

Fig. 5.   Leading-edge-jet effect[6].

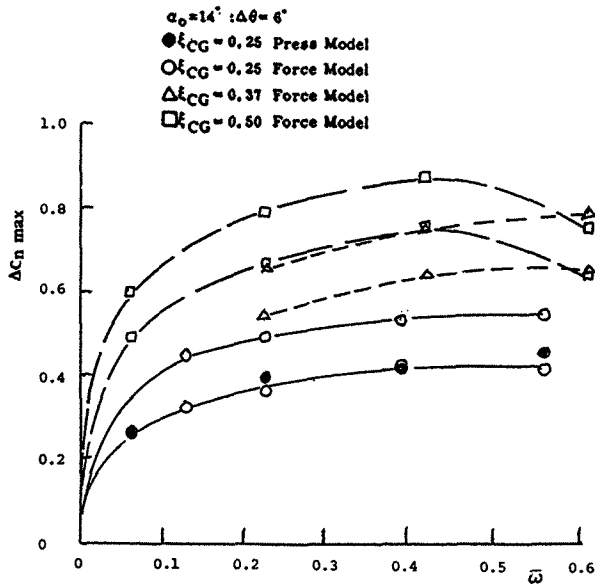Fig. 6.   Effect of rotation center location on dynamic stall overshoot of c_{nmax} (Ref. 8).

1158

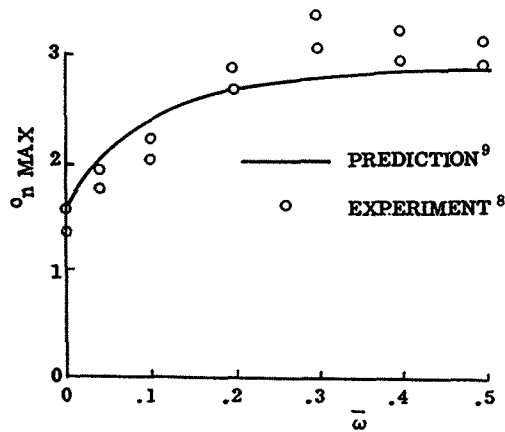Fig. 7.   Variation of $\Delta c_{n\,max}$ with $\bar{\omega}$ for the NACA-0012 airfoil[7].

Fig. 8.   Variation of $c_{n\,max}$ with $\bar{\omega}$ for the NACA-0012 airfoil, $\xi_{CG} = 0.25$ and $\Delta\theta = 10^\circ$.
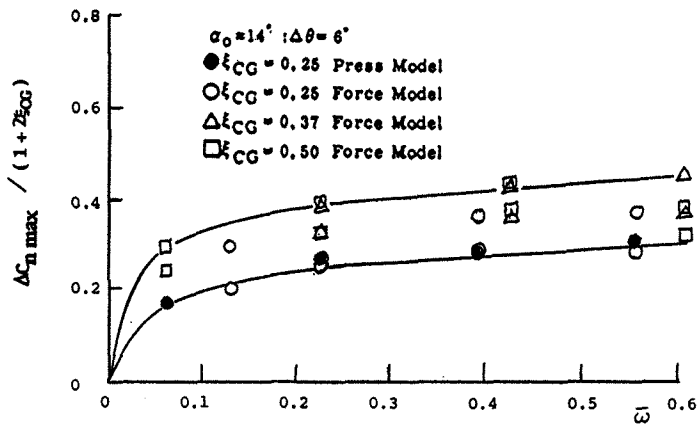
Fig. 9.   Variation of $\Delta c_{n\,max}/(1 + \xi_{CG})$ with $\bar{\omega}$ for the NACA-0012 airfoil[7].
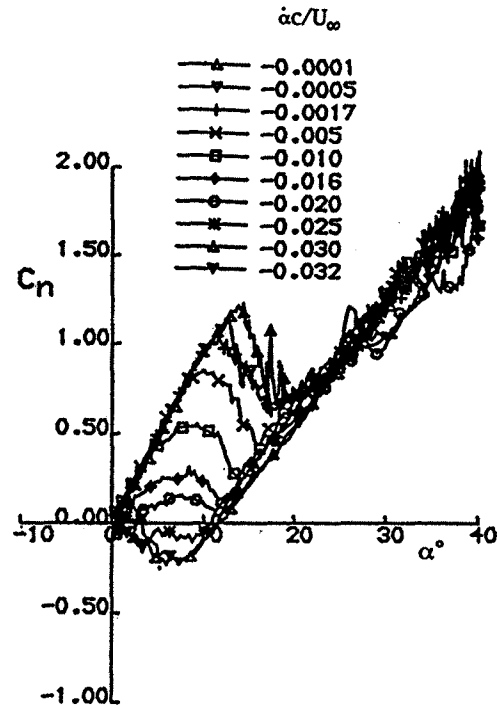
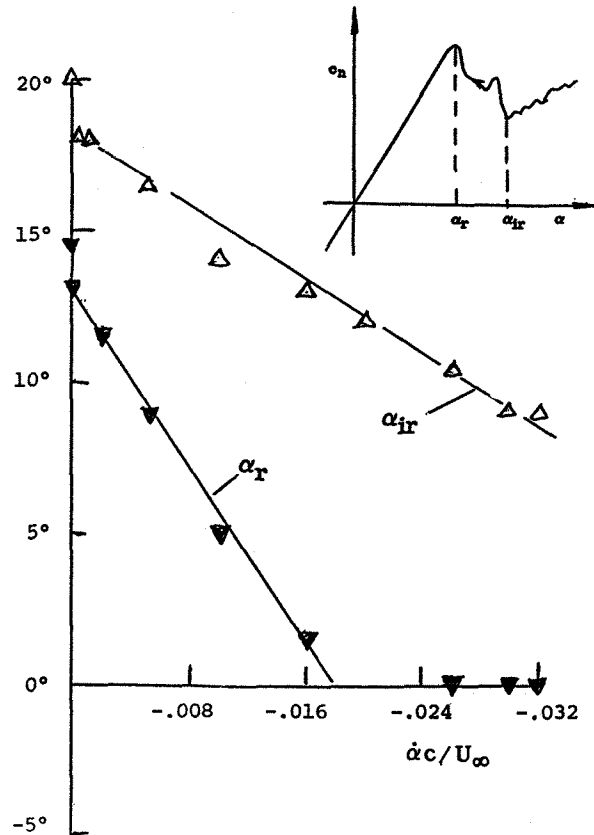Fig. 10.   Effect of dimensionless pitch rate $\dot{\alpha}c/U_\infty$ on dynamic undershoot of static flow reattachment for the NACA-0015 airfoil.

Fig. 11.   Dynamic undershoot of static flow reattachment as a function of $\dot{\alpha}c/U_\infty$ for the NACA-0015 airfoil[1].
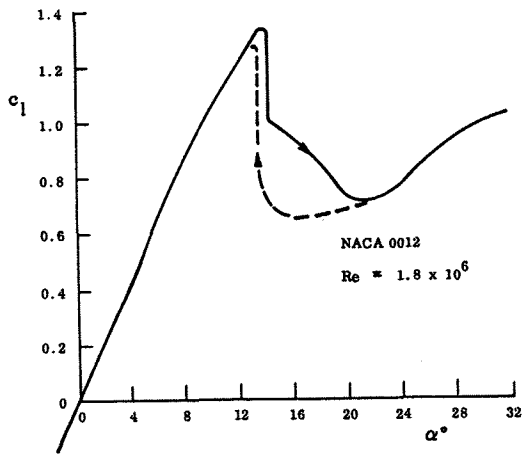
1159

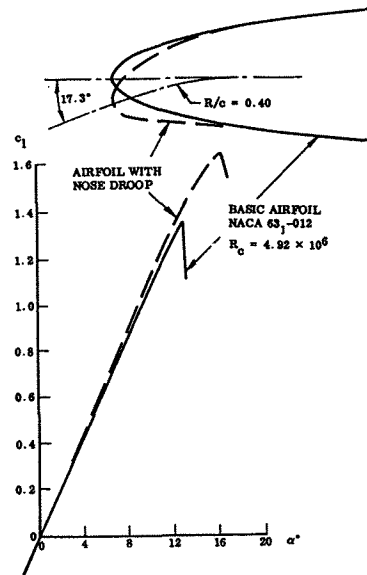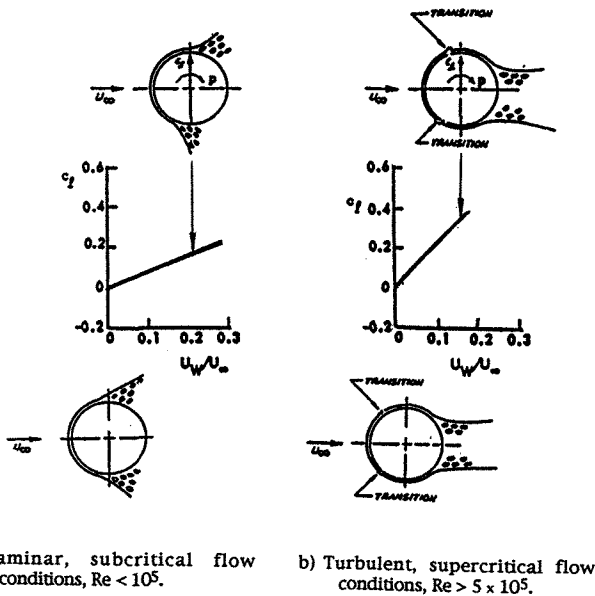Fig. 12. Static α-hysteresis for the NACA-0012 airfoil[11].

a) Laminar, subcritical flow conditions, $Re < 10^5$.

b) Turbulent, supercritical flow conditions, $Re > 5 \times 10^5$.
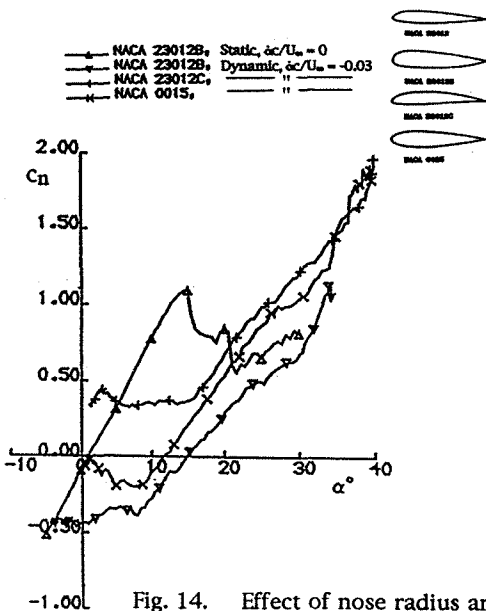
Fig. 13. Magnus lift characteristics of a circular cylinder[12].

Fig. 14. Effect of nose radius and camber on dynamic flow reattachment[1].

Fig. 15. Effect of nose-droop on maximum lift of the NACA 63_1-012 airfoil[16].

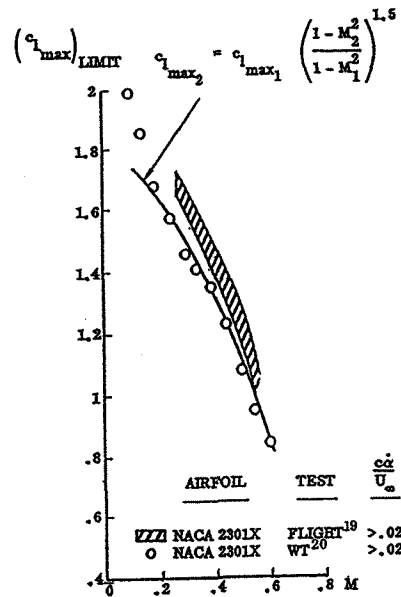$$\left(c_{l_{max}}\right)_{LIMIT} \quad c_{l_{max_2}} = c_{l_{max_1}} \left(\frac{1 - M_2^2}{1 - M_1^2}\right)^{1.5}$$

Fig. 16. Effect of compressibility on dynamic stall overshoot of maximum lift[15].

1160